Supplementary Information

Advanced Composites and Hybrid Materials

Long-range ordered graphitic structure in silk fibers delaminated using dopamine and thermal treatment for super-flexible electronic textiles

Hyun-Seok Jang,[a,#] Shinik Kim,[b,#], Ikpyeong Park,[a,#] Won Taek Jung,[a] Jong Hyeok Seo,[c] Ji-Hwan Kwon,[c] Won G. Hong,[d] Radosław Mrówczyński,[e,f] Heewoo Lee,[a] Soo Bong Choi,[a,g] Jeongwoo Kim, [a,*] Yeonho Kim,[b,*] Byung Hoon Kim [a,g,h,*]

[a] Department of Physics, Incheon National University, Incheon, 22012, Republic of Korea.

[b] Department of Applied Chemistry, Konkuk University, Chungju, 27478, Republic of Korea.

[c] Korea Research Institute of Standards and Science, Daejeon, 34133, Republic of Korea.

[d] Research Center for Materials Analysis, Korea Basic Science Institute, Daejeon, 34133, Republic of Korea.

[e] Faculty of Chemistry, Adam Mickiewicz University, Uniwersytetu Poznańskiego 8, 61-614 Poznań, Poland

[f] Centre for Advanced Technologies, Adam Mickiewicz University in Poznań, Uniwersytetu Poznańskiego 10, 61-614 Poznań, Poland.

[g] Intelligent Sensor Convergence Research Center, Incheon National University, Incheon, 22012, Republic of Korea.

[h] Institute of Basic Science, Incheon National University, Incheon, 22012, Republic of Korea.

[*] Corresponding author. E-mail address: kbh37@inu.ac.kr (Byung Hoon Kim); yeonho@kku.ac.kr (Yeonho Kim); kjwlou@inu.ac.kr (Jeongwoo Kim).

The PDF file includes:

Figure S1 to S28

Table S1 to S4

References [S1]-[S7]

Other Supplementary Materials for this manuscript include the following:

Movie S1 to S6

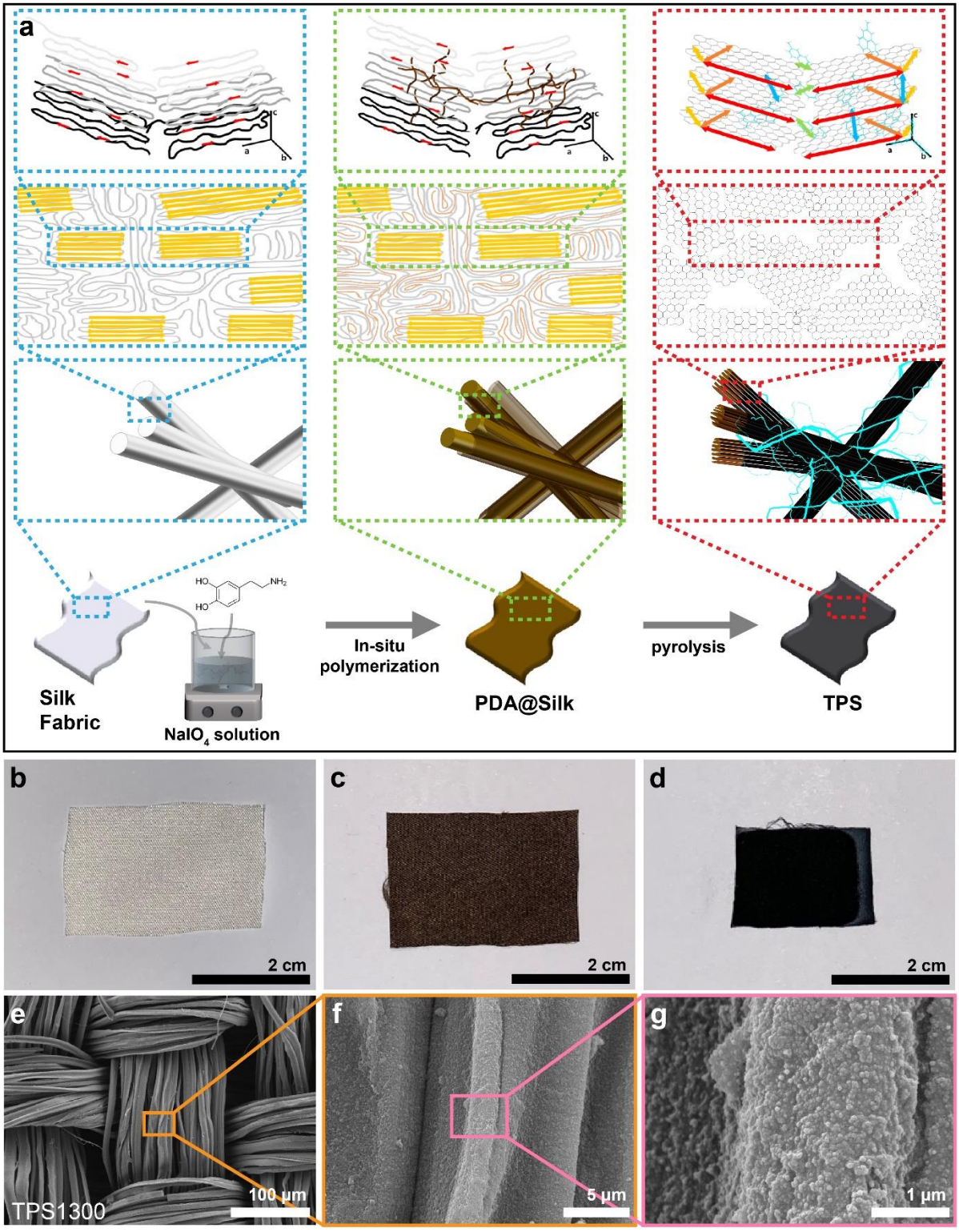

Fig. S1 Fabrication procedure and structure of TPS. **a** Scheme of the fabrication process of TPS. Optical images of **b** pristine silk fabric, **c** PDA-embedded silk fabric, and **d** TPS1300. **e** SEM image of TPS1300. **f** and **g** Magnified SEM images of (e). The aggregated PDA particles were observed on the surface of silk

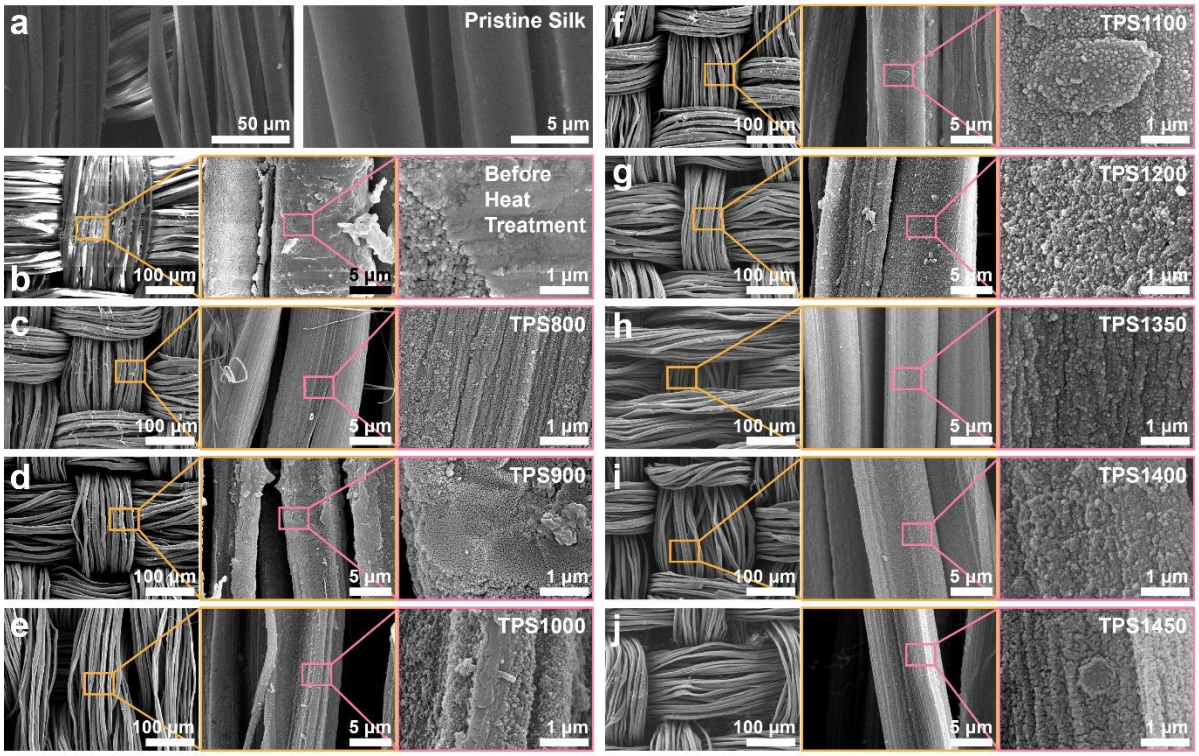

Fig. S2 Change in surface morphology of TPS with respect to HTT. SEM images of **a** pristine silk, **b** PDA-embedded silk, and **c** to **j** TPS800, TPS900, TPS1000, TPS1100, TPS1200, TPS1350, TPS1400 and TPS1450, respectively

Compared to the surface of pristine silk (Fig. S2a), before heat treatment, large-size particles and plate-like PDA were observed (Fig. S2b). While relatively small particles were found in TPS800 (Fig. S2c). The particle size increased with an HTT higher than 800 °C, resulting in aggregation due to thermal energy (Fig. S1e-g and Fig. S2c-j). The electrical conductivity of TPS originated from the simultaneous carbonization of PDA and silk through heat treatment. Before determining the electrical characteristics, we used a scanning electron microscope (SEM) to investigate the structural changes of the silk caused by the PDA.

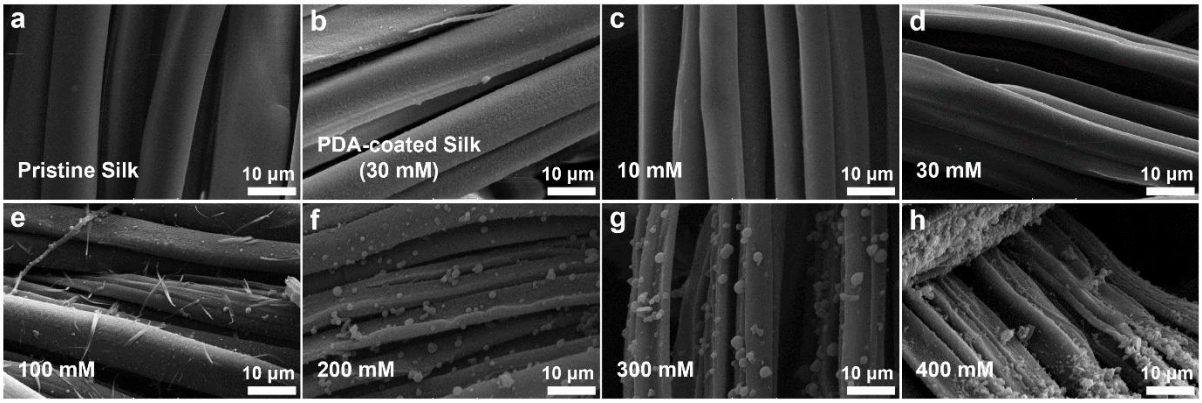

Fig. S3 Side view of the delaminated TPS900 depending on molarity. SEM images of **a** pristine silk, **b** PDA-embedded silk (30 mM of PDA) before heat treatment, **c** to **h** TPS900 synthesized using the different molar concentrations of PDA, 10, 30, 100, 200, 300, and 400 mM, respectively

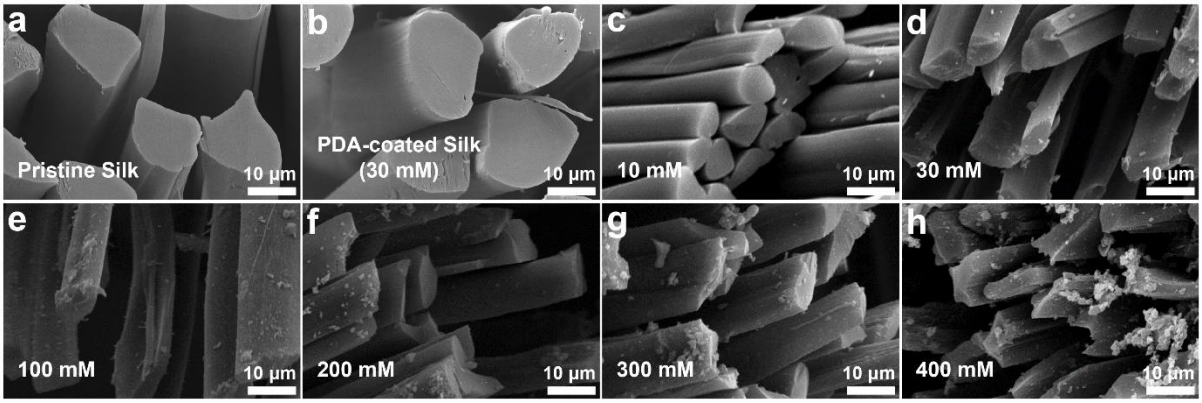

Fig. S4 Cross-section of the delaminated TPS900 depending on molarity. SEM images of **a** pristine silk, **b** PDA-embedded silk (30 mM of PDA) before heat treatment, **c** to **h** TPS900 synthesized using the different molar concentrations of PDA, 10, 30, 100, 200, 300, and 400 mM, respectively

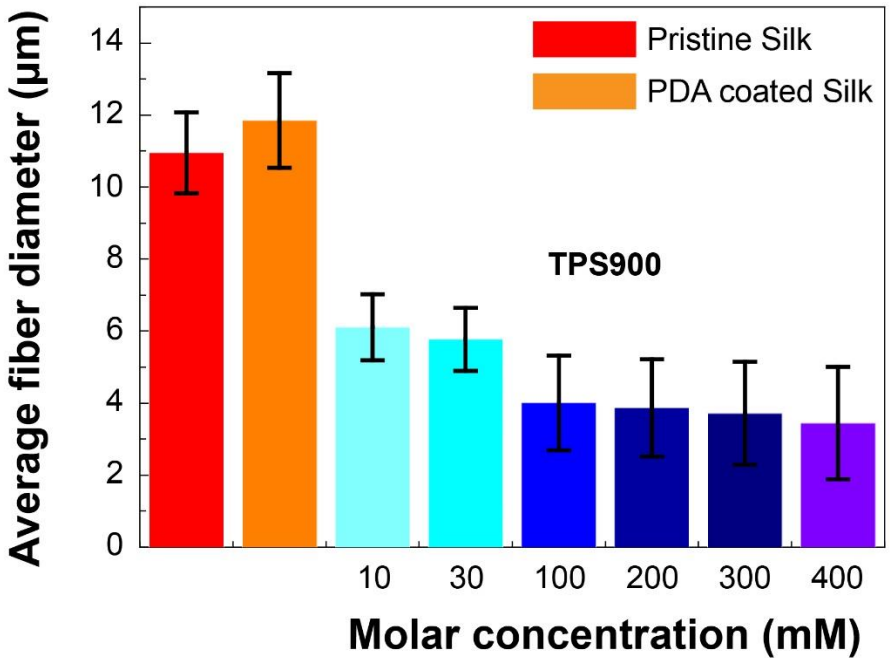

Fig. S5 Molar concentration-dependent diameter variation. The average diameters (or width) decreased with an increase in the molar concentration of PDA

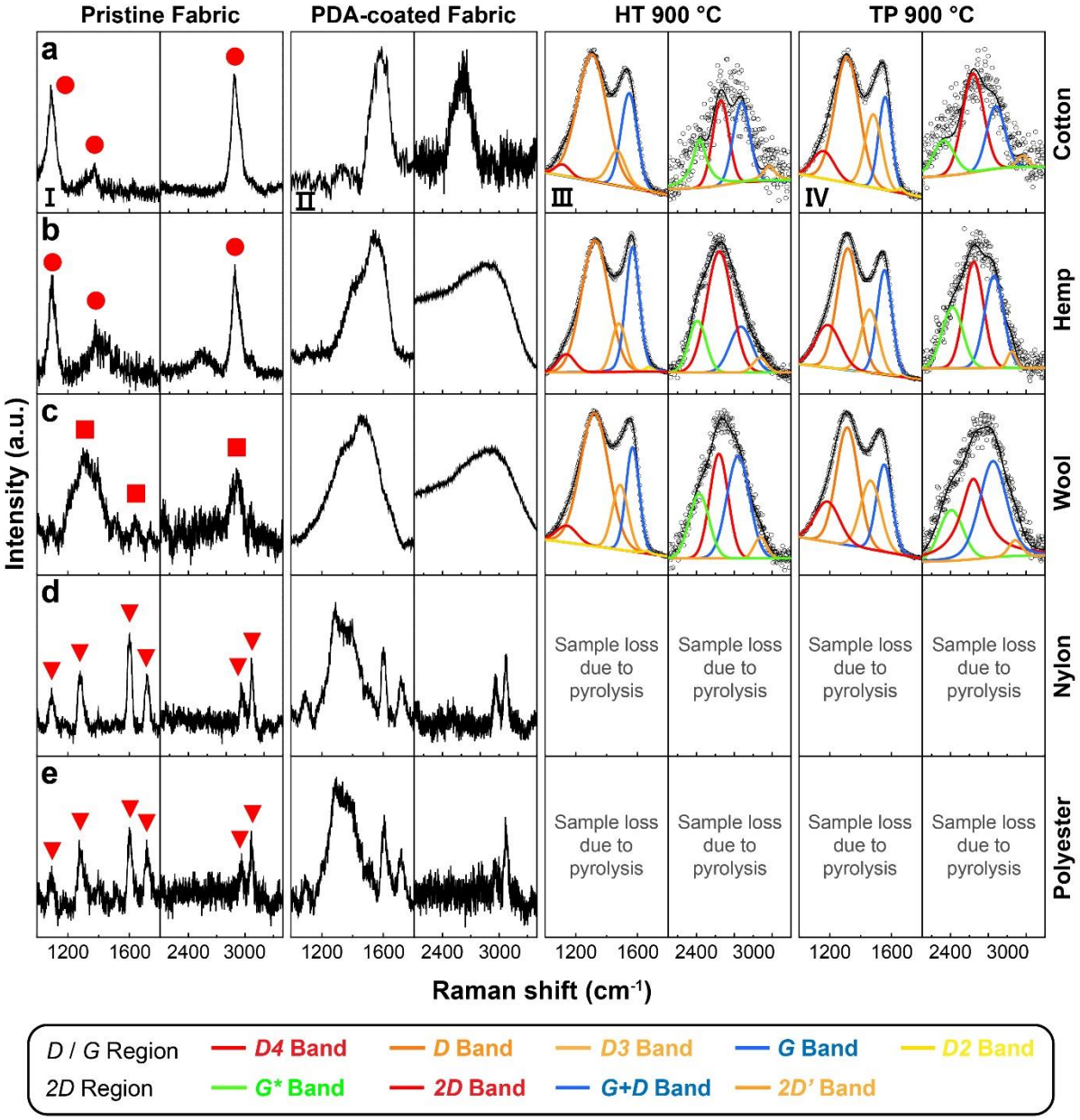

Fig. S6 Comparison of structural transition of other textiles with Raman spectroscopy. The row and column of the figure represent the type of textiles and sample manipulation conditions, respectively. HT 900 °C means the heat treatment at 900 °C. TP 900 °C indicates PDA-embedded textiles treated at 900 °C. Raman spectra of **a** cotton, **b** hemp, **c** wool, **d** nylon, and **e** polyester

Figure S6a(I) and b(I) shows that the peaks in Raman spectra for cotton and hemp (red circles) are typical characteristics of cellulose [S1]. The peaks centered near 1270, 1654, and 3000 cm^{-1} (red squares) correspond to amide III, I, and C-H stretching modes in wool (Fig. S6c(I)) [S2]. In the case of nylon and polyester, C-C stretching, amide I, III, and CH_2 bending modes were

well defined (Fig. S6d(I) and e(I), inverted triangles) [S3]. Relatively broad peaks were observed in PDA-embedded textiles (Fig. S6(II)), which came from the Raman bands of PDA. Nylon and polyester fabrics were burnt out after heat treatment at 900 °C, unlike natural sources (cotton, hemp, and wool). *D*, *D2*, *D3*, *D4*, and *G* bands in the range 1200 - 1600 cm^{-1} and *G**, *2D*, *G+D*, and *2D'* bands in 2400 – 3200 cm^{-1} were observed in heat-treated (HT) pristine textiles as well as thermally treated PDA-embedded (TP) cotton, TP hemp, and TP wool. Although it shows the possibility to use them for e-textiles, the flexibility is not even close to the TPS. It will be discussed in the bending cycle-dependent resistance.

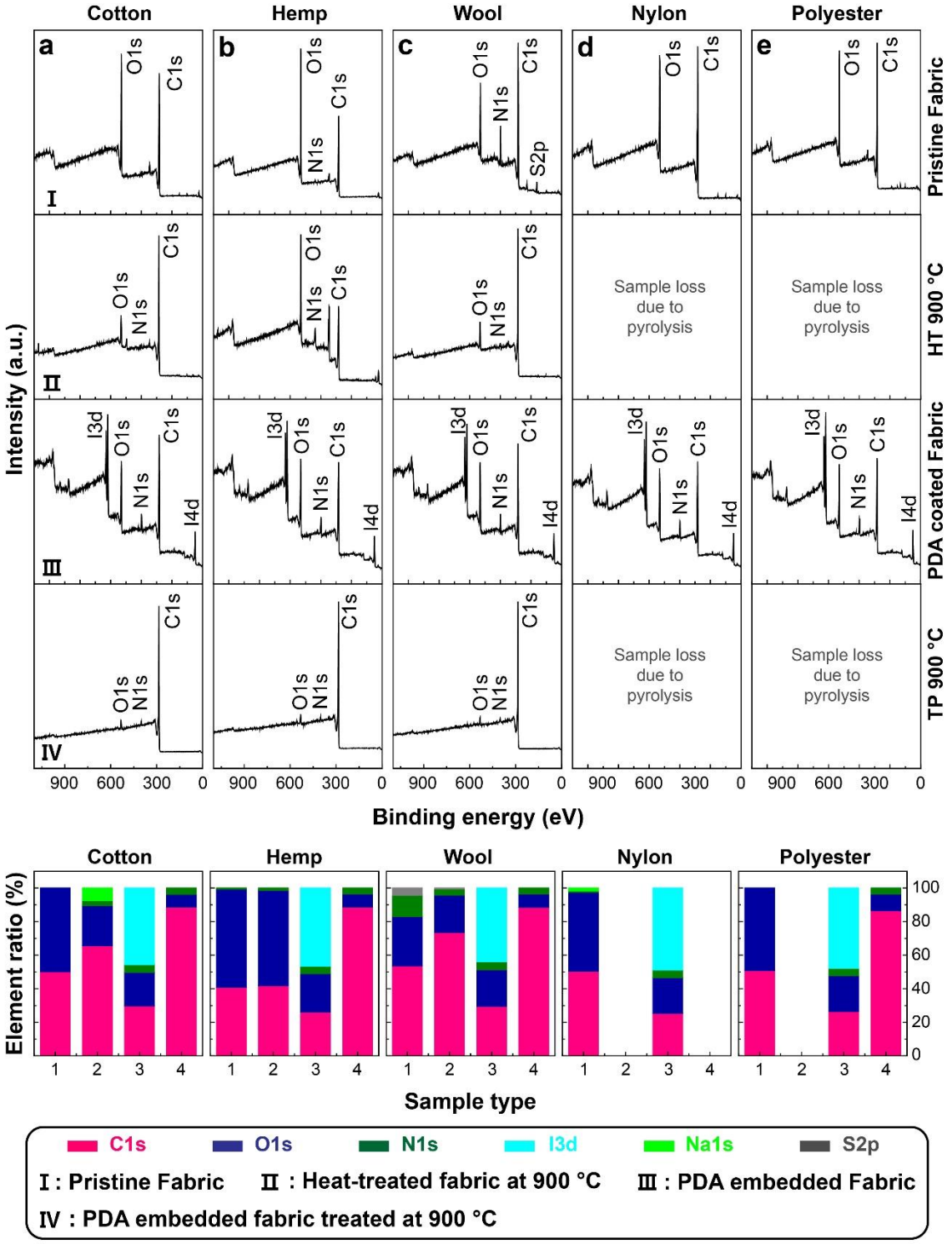

Fig. S7 Comparison of structural transition of other textiles with XPS. The column and row of the figure represent the type of textiles and sample manipulation conditions, respectively. XPS survey spectra of **a** cotton, **b** hemp, **c** wool, **d** nylon, and **e** polyester. All textiles show a decrease in oxygen and nitrogen species due to the heat treatment

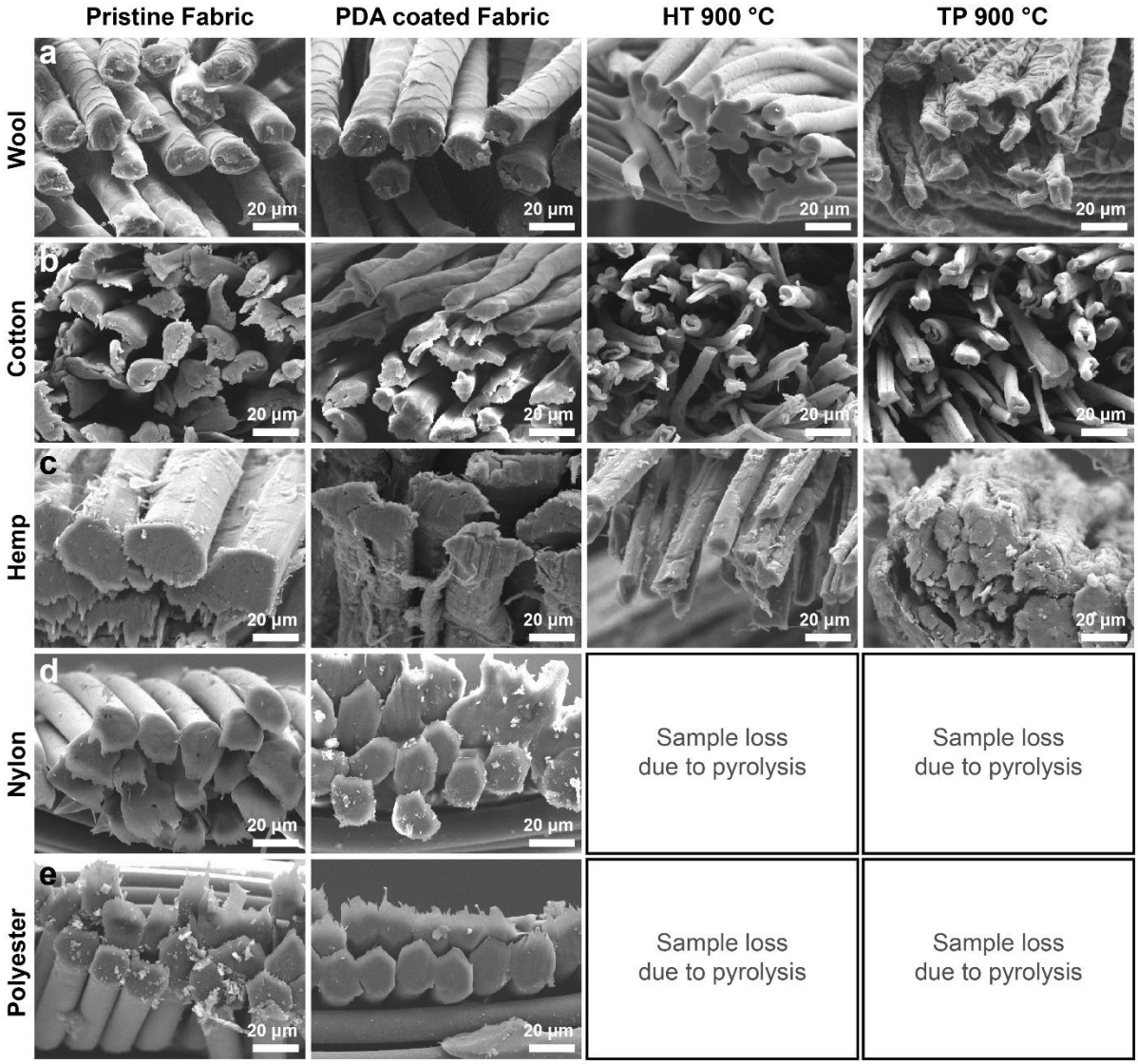

Fig. S8 Cross-sectional SEM images of other textiles**. a** wool, **b** cotton, **c** hemp, **d** nylon, and **e** polyester

Figures S8 and S9 are SEM images of wool, cotton, hemp, nylon, and polyester. Due to PDA coating, the diameters of the fibers became larger compared with the pristine textiles. After heat treatment at 900 °C, the fibers in the pristine textiles were shrunk, and some fibers melted and clumped together (wool and hemp). As mentioned above, nylon and polyester were burnt out. The helix structure was observed in the heat-treated cotton. For TP cotton, relatively unwound fibers were found. The fibers of TP wool (TP900) were shrunk but the shape was maintained. TP hemp fibers seemed to be melted and aggregated.

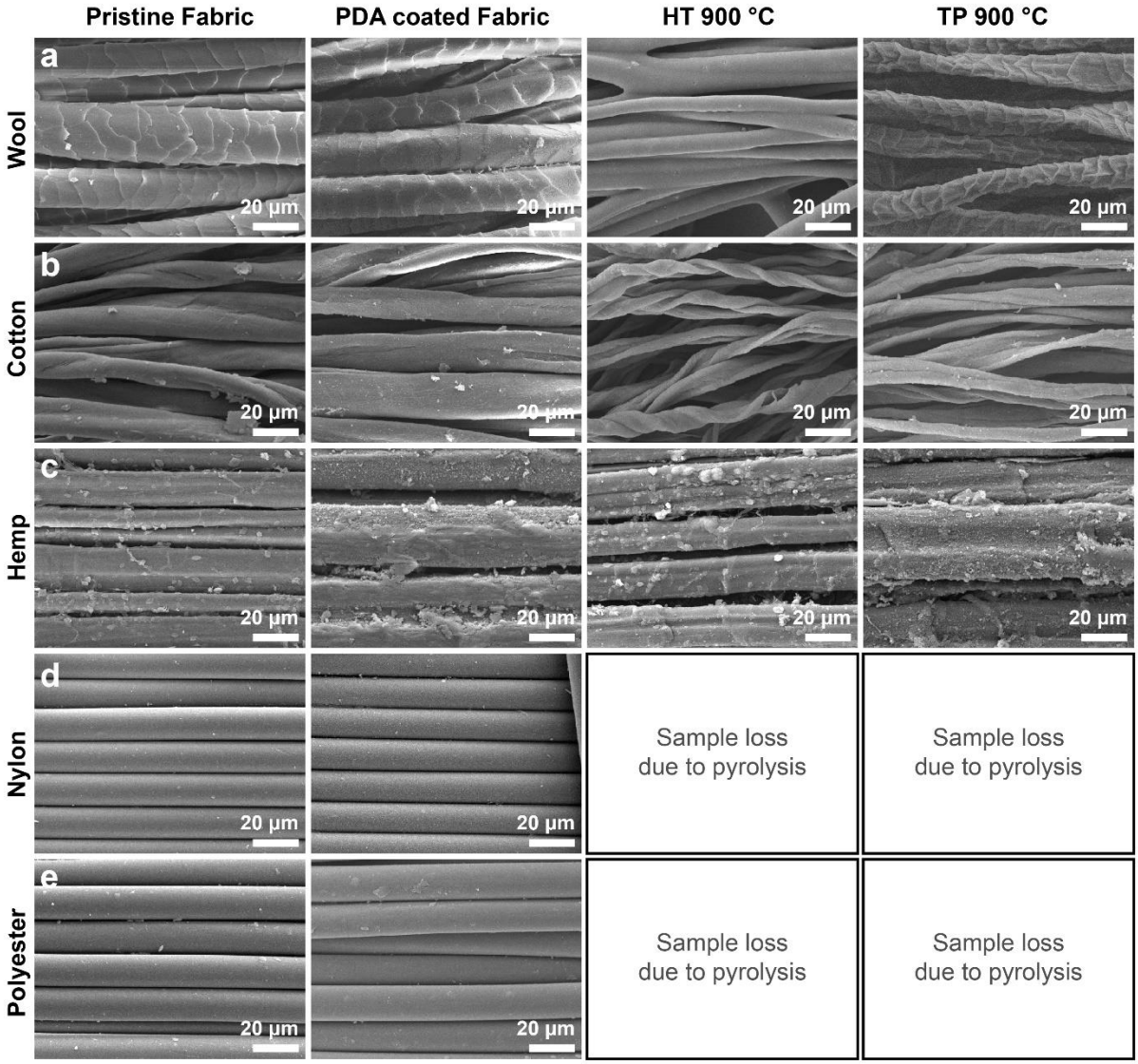

Fig. S9 Side view SEM images of other textiles. **a** wool, **b** cotton, **c** hemp, **d** nylon, and **e** polyester

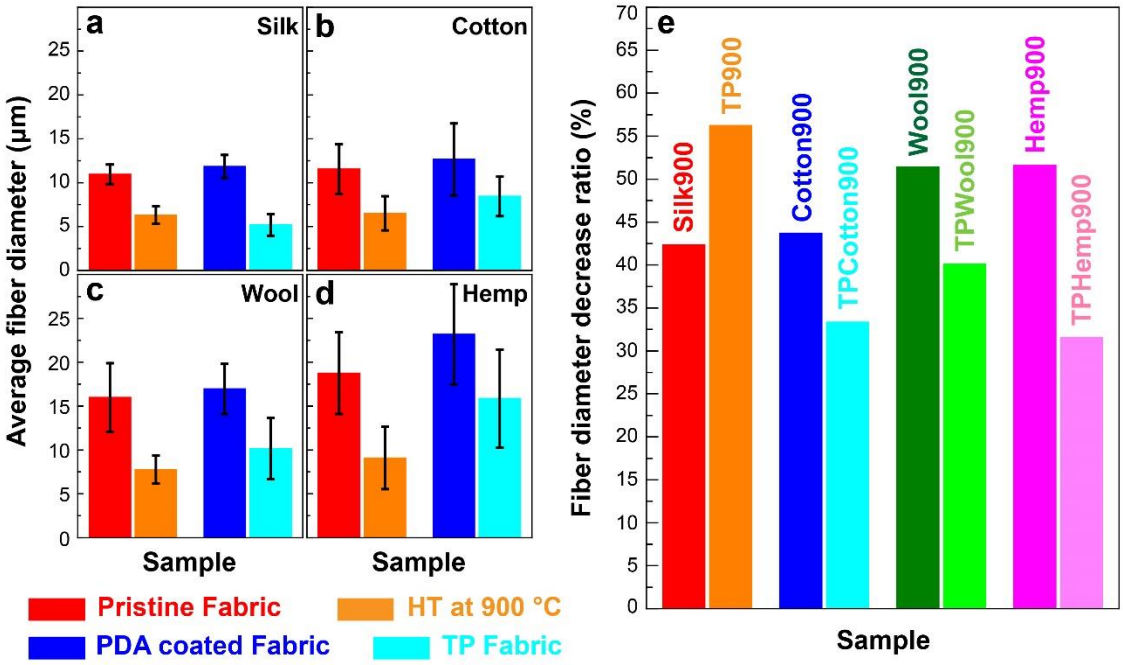

Fig. S10 Fiber diameters. Variation of the fiber diameters of **a** silk, **b** cotton, **c** wool, and **d** hemp due to heat treatment at 900 °C. **e** Comparison of diameter change between heat-treated pristine fibers and PDA-embedded (or coated) fibers. 900 means the heat treatment at 900 °C

The fiber diameter change caused by heat treatment at 900 °C is depicted in Fig. S10. We chose the fibers thermally treated at 900 °C because it was the highest temperature to have the flexibility of wool and cotton. Pristine (P) silk and PDA-embedded (Pe) silk showed 42.4% and 56.2% decrease in diameter, respectively (Fig. S10a). On the contrary, the decreased ratio in the fibers of Pe-cotton, -wool, and -hemp is small compared with P-cotton, -wool, and -hemp (Fig. S10b-e, and Table S1).

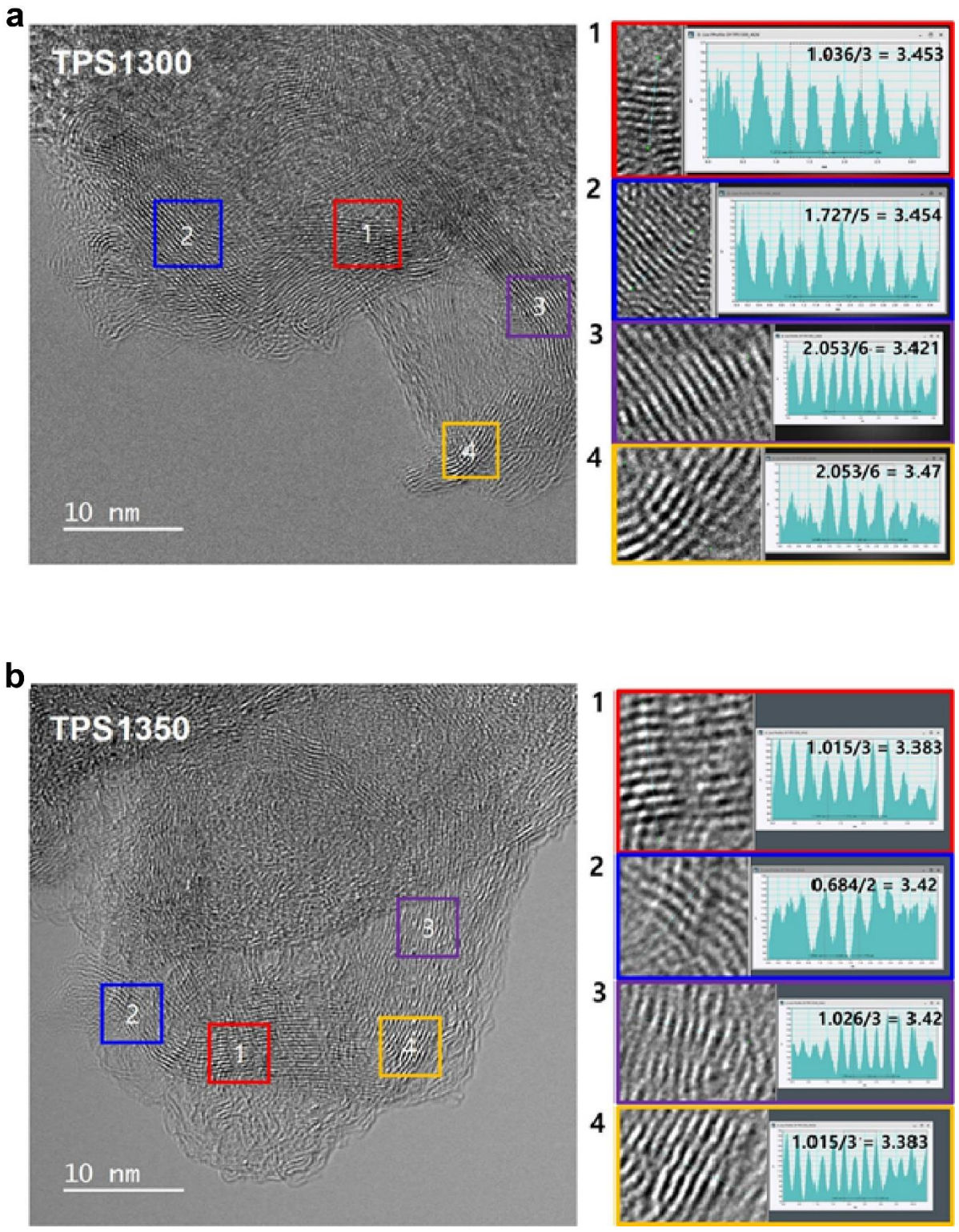

Fig. S11 TEM images and the measured lattice distance. Randomly measured 4 spots in TEM images and the calculated average value to determine lattice distance of each sample. **a** TPS1300 and **b** TPS1350

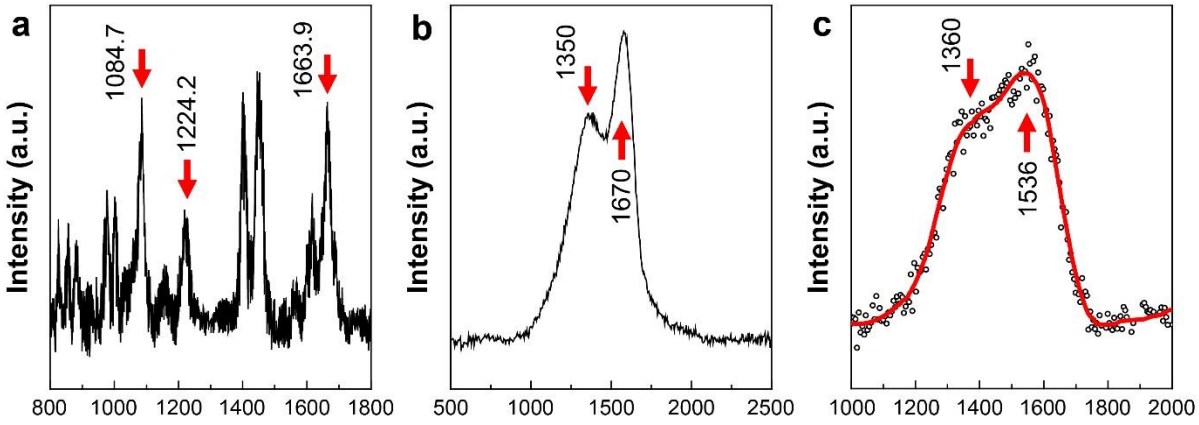

Fig. S12 Raman spectra of **a** pristine silk, **b** PDA, and **c** PDA-embedded silk. The peaks centered at 1084.7, 1224.2, and 1663.9 cm^{-1} are characteristic of silk (Fig. S12a) [S4]. PDA consists of carbon atoms and functional groups. Hence *D* and *G* bands were observed in the Raman spectrum (Fig. S12b). The relatively broad peaks compared with PDA were found in PDA-embedded silk (Fig. S12c), which is attributed to the merging of Raman bands from silk and PDA

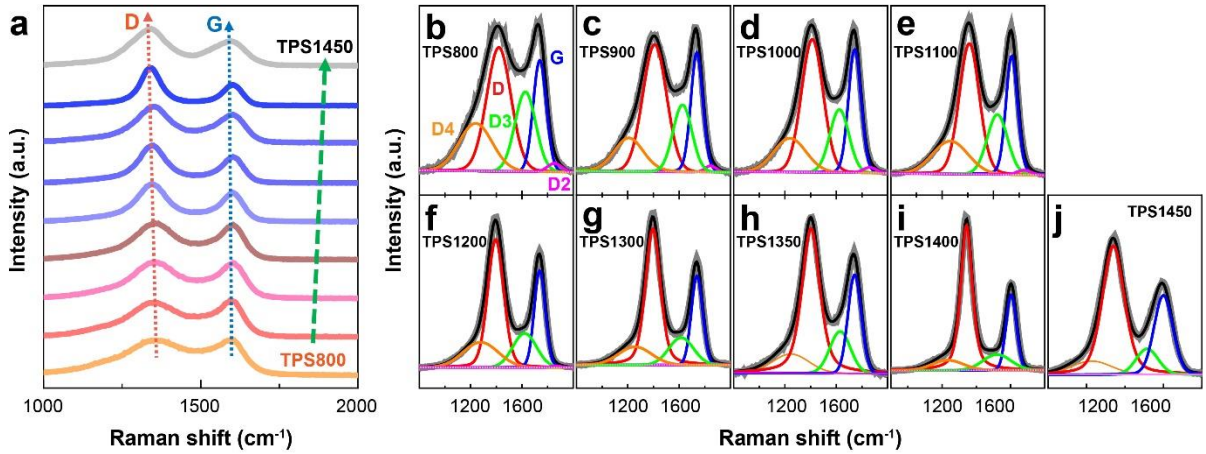

Fig. S13 Raman spectroscopy of TPS. **a** Evolution of *D* and *G* bands with the increase of HTT. As HTT increases, both peaks become prominent and I_D/I_G ratio increases. To show this property systematically, we compared both peaks (deconvoluted to five peaks) with respect to HTT. The variation of *D*, D_2, D_3, D_4, and *G* bands of **b** TPS800, **c** TPS900, **d** TPS1000, **e** TPS1100, **f** TPS1200, **g** TPS1300, **h** TPS1350, **i** TPS1400, and **j** TPS1450. D_2 band near 1690 cm^{-1} indicates that TPSs are highly defective structures. D_4 and D_3 bands near 1220 and 1520 cm^{-1} can be interpreted by disordered amorphous carbons [S5]

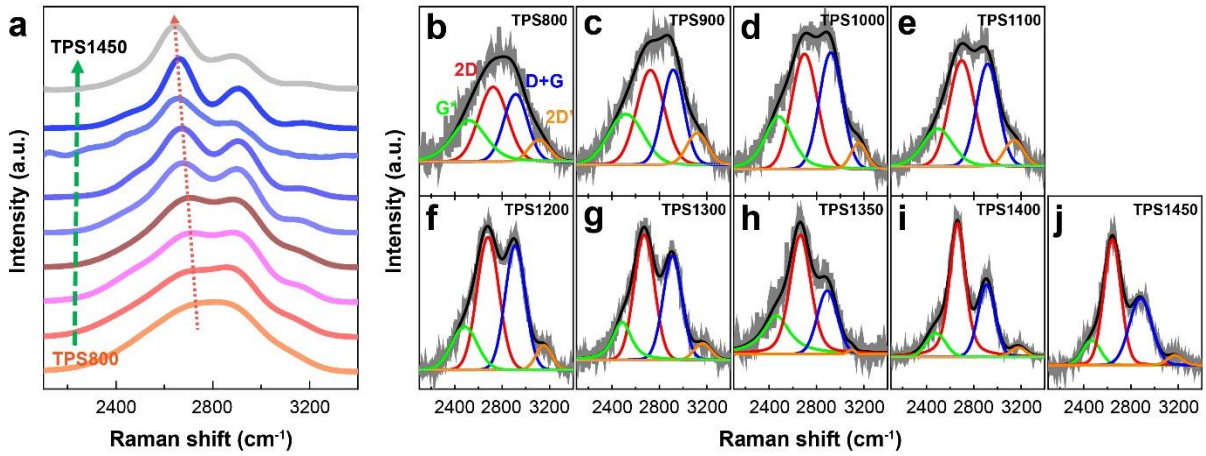

Fig. S14 Variation of *2D*-related bands in Raman spectroscopy of TPS. **a** Change in peaks near 2800 cm^{-1} (the deconvoluted four bands, *G**, *2D*, *D+G*, and *2D′*). *G**, *D+G*, and *2D′* peaks are present in materials with lots of defects. *2D* and *D+G* peaks are prominent but the other two peaks decrease. The change of these bands for **b** TPS800, **c** TPS900, **d** TPS1000, **e** TPS1100, **f** TPS1200, **g** TPS1300, **h** TPS1350, **i** TPS1400, and **j** TPS1450 with the increase of HTT

The *D* and *G* bands were composed of the first-order bands of *G*, *D(D1)*, *D2*, *D3*, and *D4* (Fig. S13). As HTT increased, the defect-related bands *D2*, *D3*, and *D4* significantly decreased. Finally, the *D* and *G* bands became predominant and the FWHMs decreased (Table S2). This behavior was also observed in the *2D* region, which was deconvoluted in four bands, *G**, *2D(G′)*, *D+G*, and *2D′* [S6] (Fig. S14). Of note, the *2D* band usually found in graphene and graphite became prominent and red-shifted from 2725 cm^{-1} for TPS800 to 2658 cm^{-1} for the TPS1450 like *D* peak.

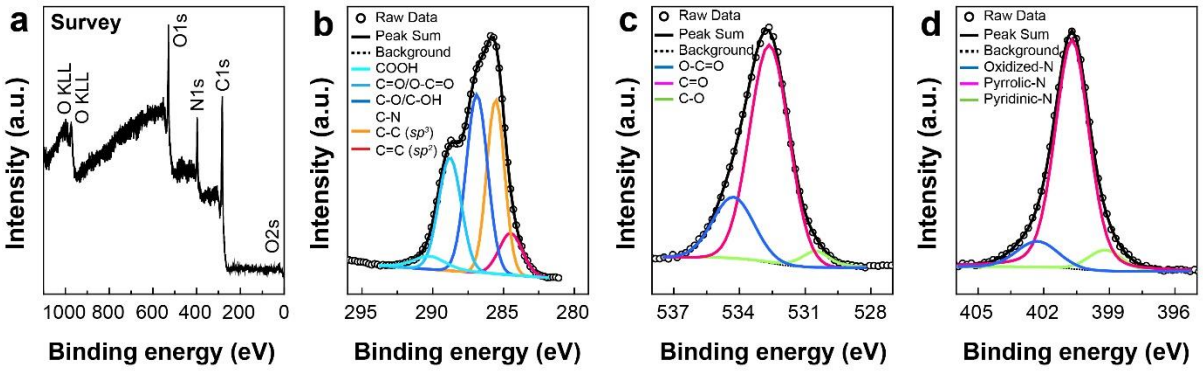

Fig. S15 XPS spectra of pristine silk. **a** Survey for entire peaks. High-resolution **b** C1s, **c** O1s, and **d** N1s spectra

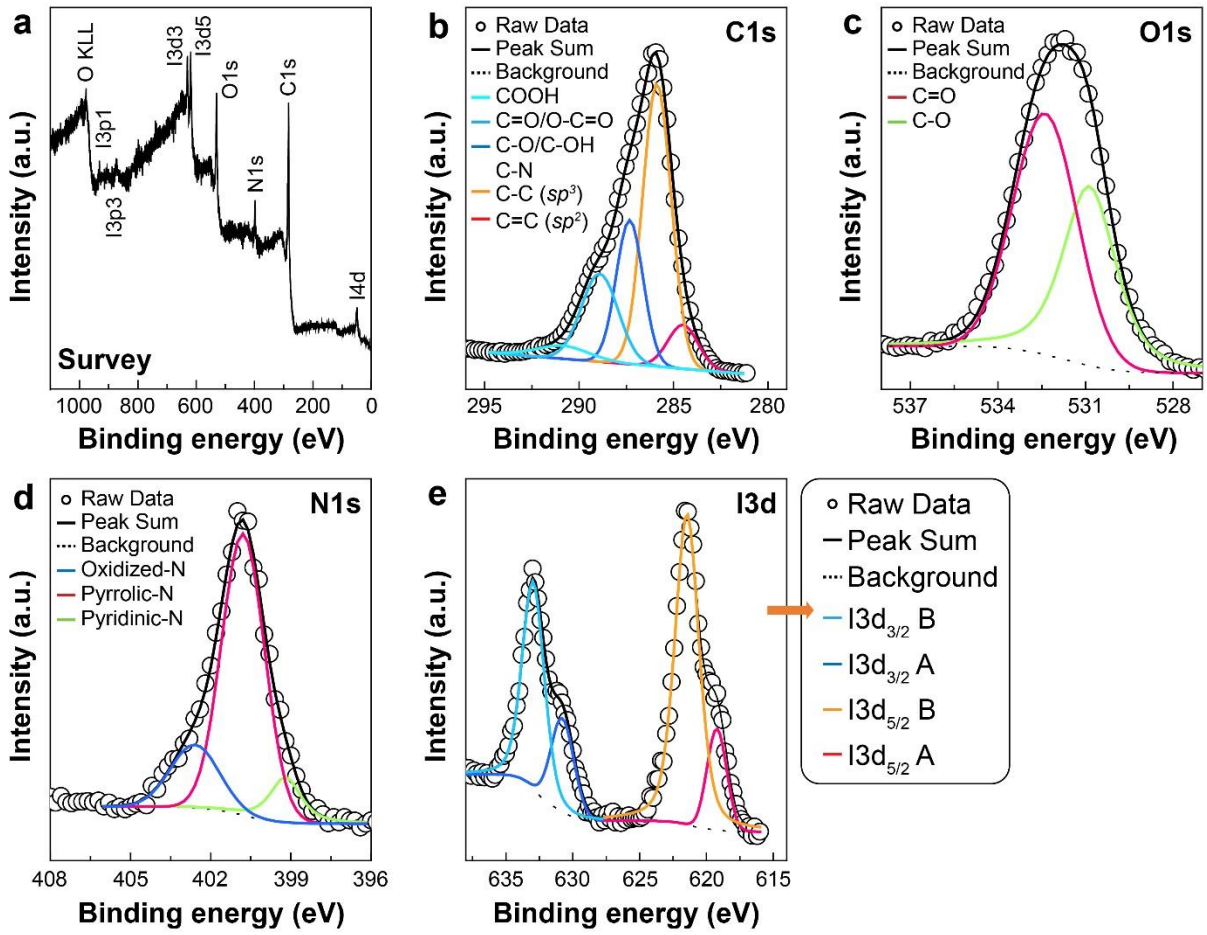

Fig. S16 XPS spectra of PDA-embedded silk before heat treatment. **a** Survey for entire peaks. High-resolution **b** C1s, **c** O1s, **d** N1s, and **e** I3d spectra. Iodine comes from the process of polymerization of dopamine

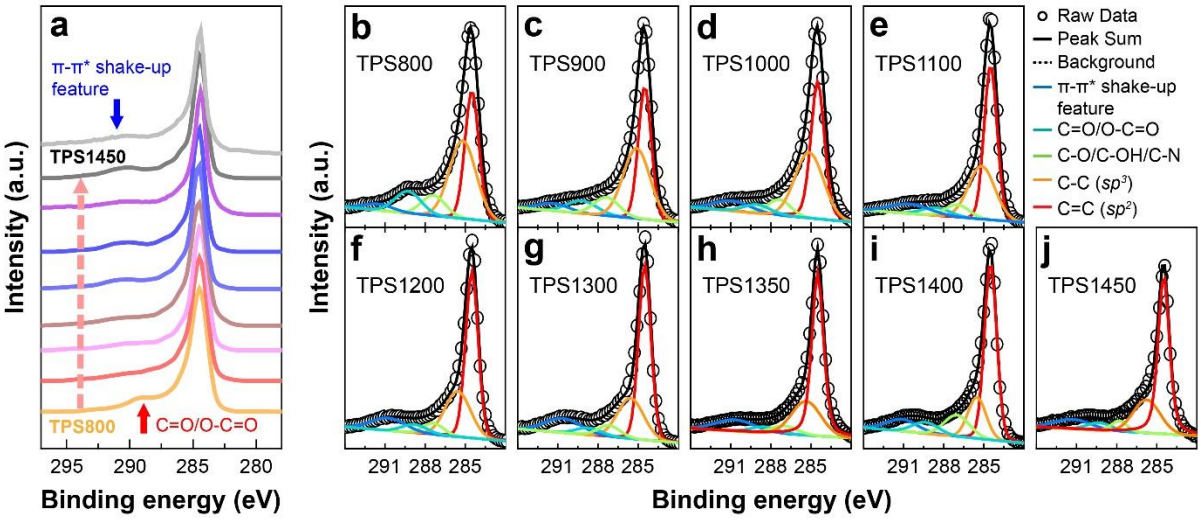

Fig. S17 C1s XPS spectra of TPS. C1s peak is composed of five peaks, C=C, C-C, C-O/C-OH/C-N, C=O/O-C=O, and π-π* shake-up feature near 284, 285, 287, 288, and 290 eV, respectively **a** HTT-dependent C1s spectra. The blue and red arrows respectively are π-π* shake-up feature and C=O/O-C=O species. The evolution of C1s spectra of **b** TPS800, **c** TPS900, **d** TPS1000, **e** TPS1100, **f** TPS1200, **g** TPS1300, **h** TPS1350, **i** TPS1400, and **j** TPS1450 as HTT increases

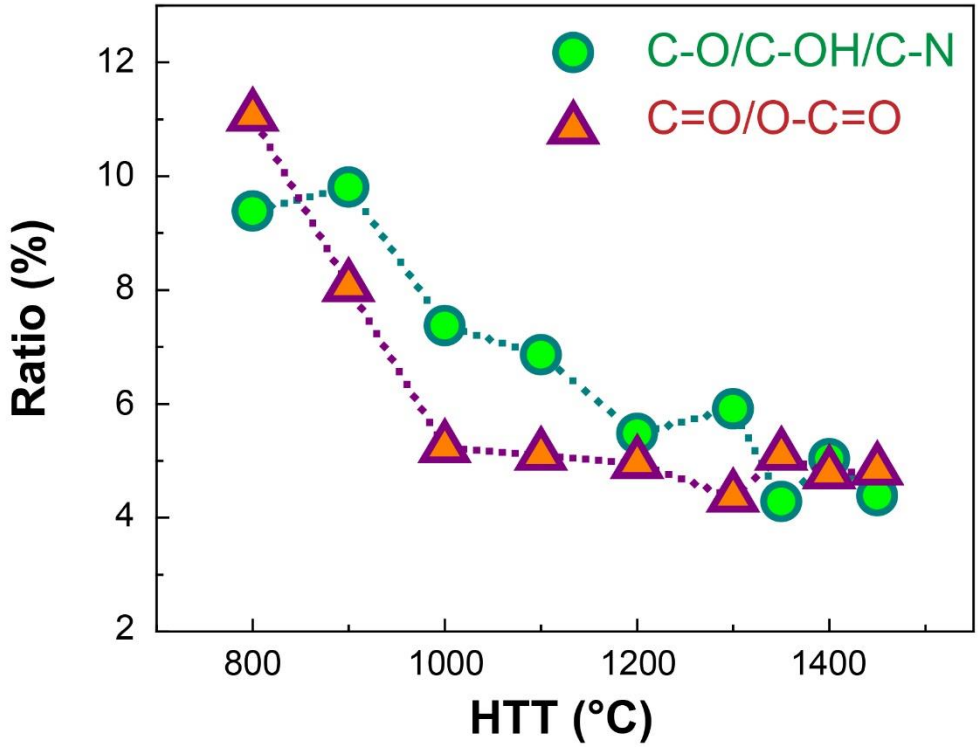

Fig. S18 HTT-dependent atomic concentration. C=O/O-C=O and C-O/C-OH/C-N species decreased with an increase of HTT

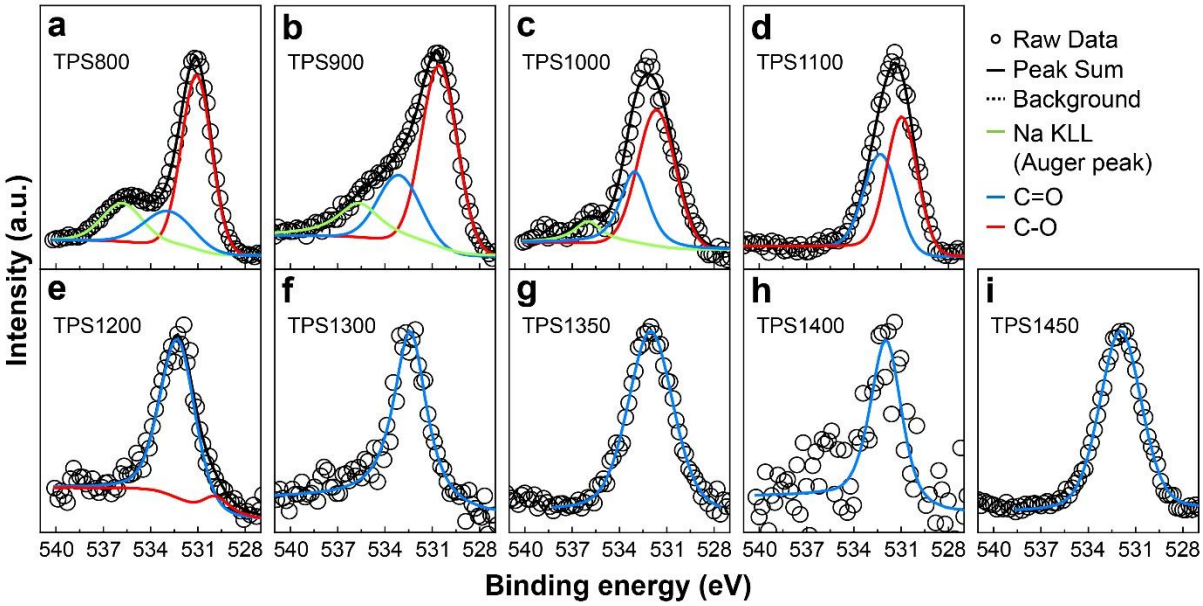

Fig. S19 XPS O1s spectra with respect to HTT. **a** TPS800, **b** TPS900, **c** TPS1000, **d** TPS1100, **e** TPS1200, **f** TPS1300, **g** TPS1350, **h** TPS1400, and **i** TPS1450. The development of Na peak (green lines) comes from the constituents used in the bleaching process of commercial silk, which disappeared when the silk was treated at 1100 °C. C-O species gradually decreased, and finally, only C=O remained in TPS heated over 1300 °C

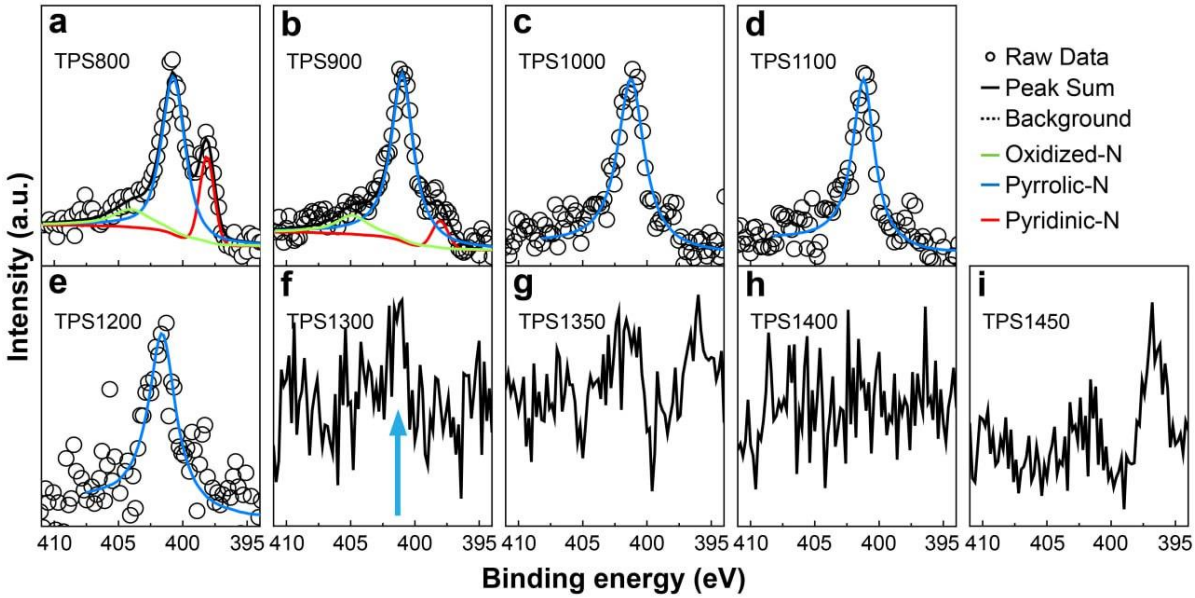

Fig. S20 XPS N1s spectra with respect to HTT. **a** TPS800, **b** TPS900, **c** TPS1000, **d** TPS1100, **e** TPS1200, **f** TPS1300, **g** TPS1350, **h** TPS1400, and **i** TPS1450. The cyan-colored arrow in Fig. S20f represents the pyrrolic-N. Peaks near 298, 401, and 404 eV are assigned to pyridinic-, pyrrolic-, and oxidized-N, respectively [S7]. These bands are clearly observed in TPS800, but pyridinic- and oxidized-N are diminished in TPS900 and disappear in TPS1000. The pyrrolic-N also vanishes in TPS1350

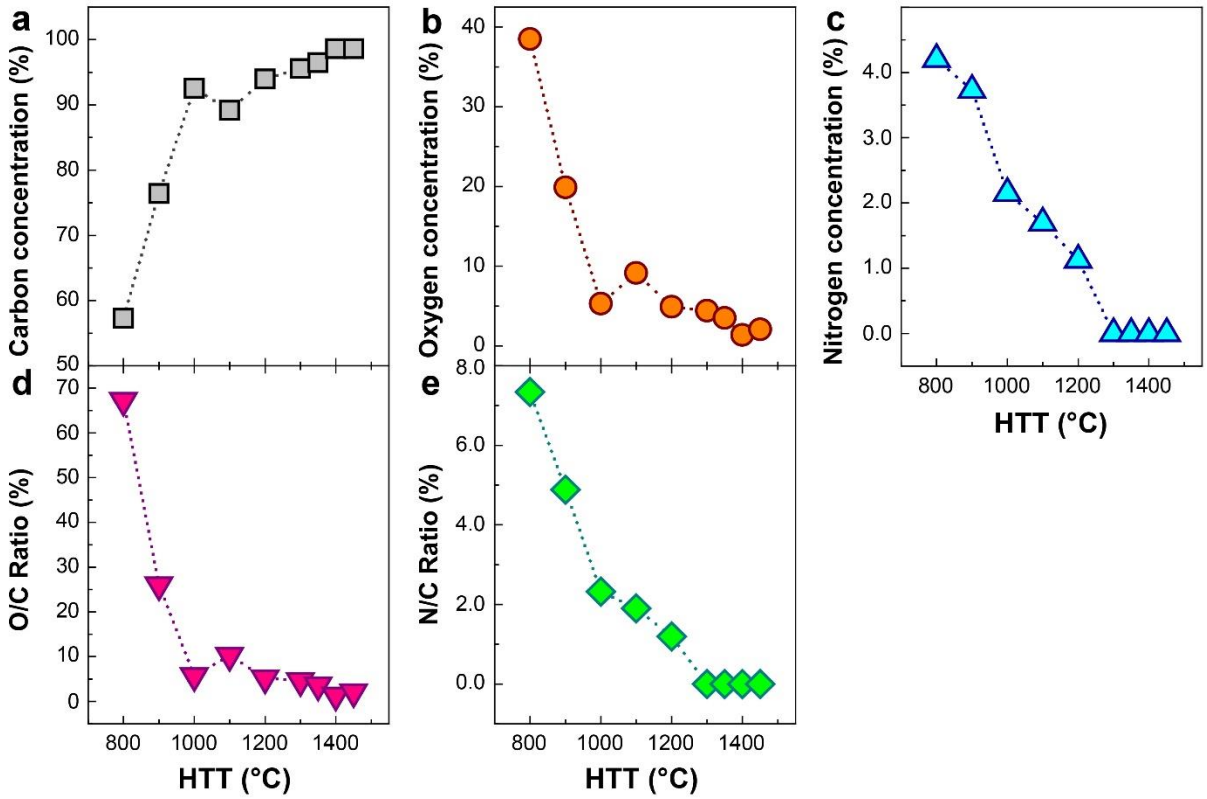

Fig. S21 Atomic concentration obtained from XPS study. Change in the concentration of **a** carbon, **b** oxygen, and **c** nitrogen atoms as a function of HTT. The overall carbon species increases but oxygen and nitrogen species decrease as HTT increases. This behavior is confirmed with **d** O/C ratio and **e** N/C ratio

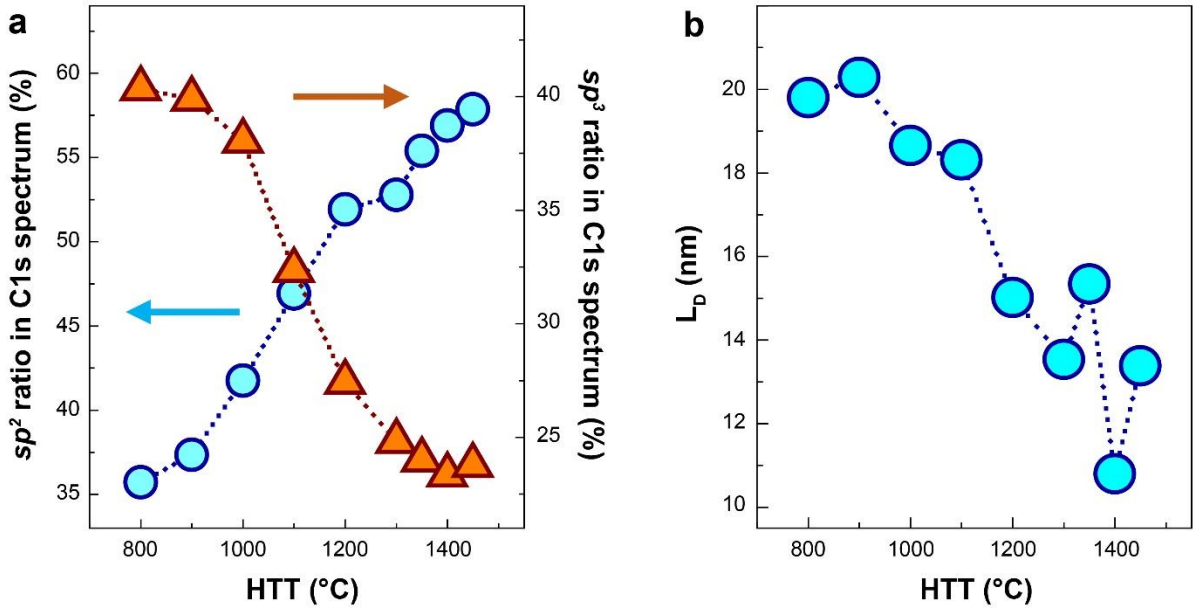

Fig. S22 Structural change of TPS. The change in amount of **a** sp^2 (cyan circles) and sp^3 (orange triangles) carbon species. **b** L_D changes as a function of HTT

The C=O/O-C=O species and π-π* shake-up feature were present with a slight hump near 289 and 291 eV, respectively (Fig. S17). The C=O/O-C=O species drastically decreased in TPS900 and TPS1000 and then decreased monotonously (orange triangles in Fig. S18). A relatively gradual reduction in the C-O/C-OH/C-N species was observed (green circles in Fig. S18), which was also observed in the O1s and N1s spectra (Figs. S19-S21, and Table S3). For the carbon species, the sp^2 carbon increased; however, the sp^3 carbon decreased with an increase in HTT (Fig. S22a).

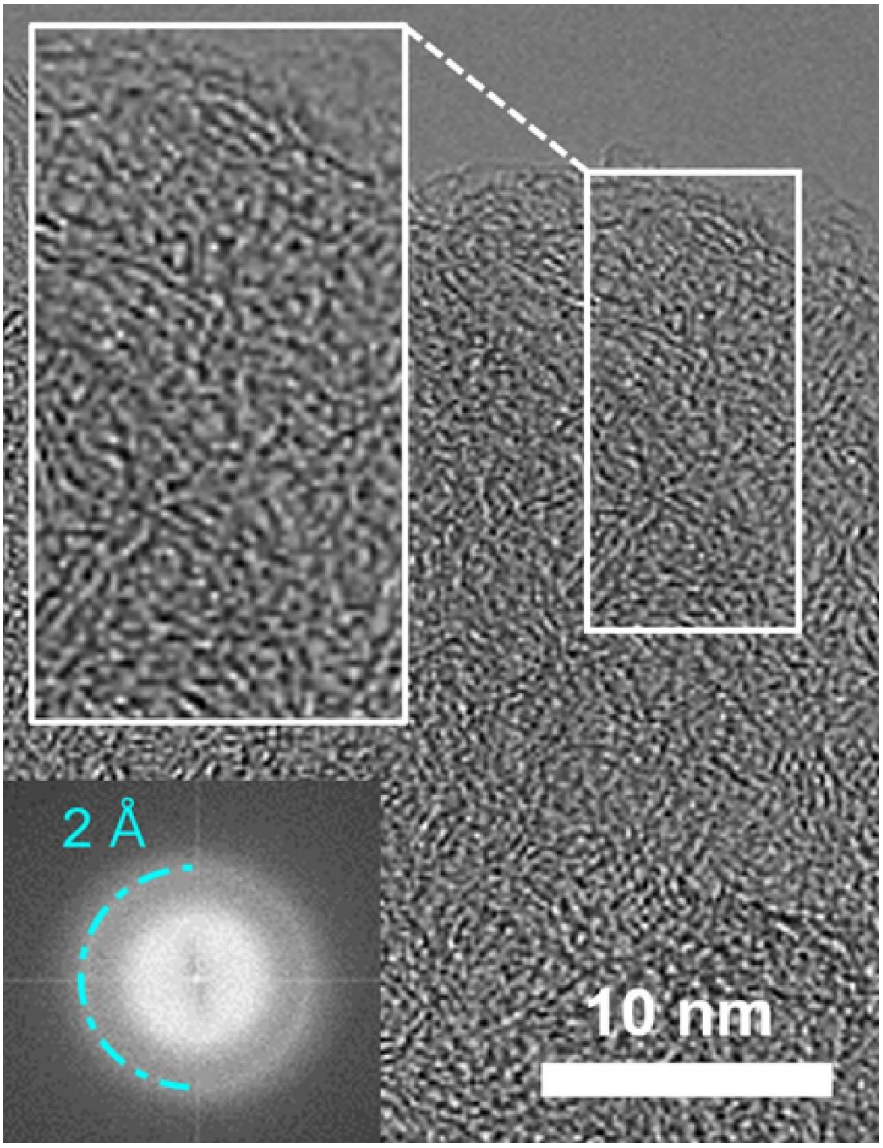

Fig. S23 Structure of Silk1300. TEM image and diffraction pattern

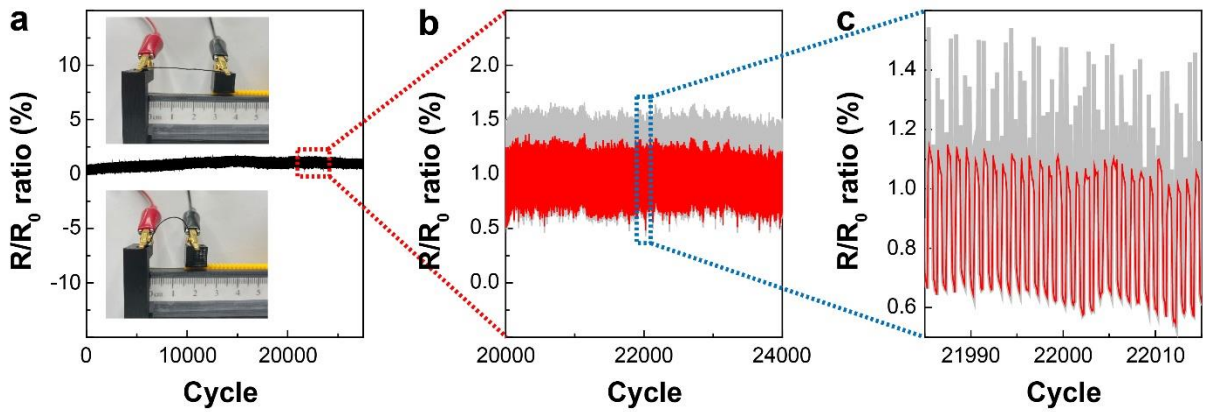

Fig. S24 Stable conducting behavior for bending. **a** The bending-cycle-dependent resistance of TPS1300 yarn over 25,000 cycles was measured using a homemade bending device (insets). The upper and lower images show stretched and bent yarns, respectively. **b** and **c** magnified graph to show more detail. The grey line is the original data. The resistance variation was less than 0.6%. The unexpected increase in R/R_0 during the stretching process was shown. It occurred from the contact between electrical holder clips and TPS yarn. We counted the unexpected increase out of the original data (red line) and then found that the R/R_0 between stretched and bent position is approximately 0.5%. The flexibility of TPS1300 is comparable with pristine (pure) silk

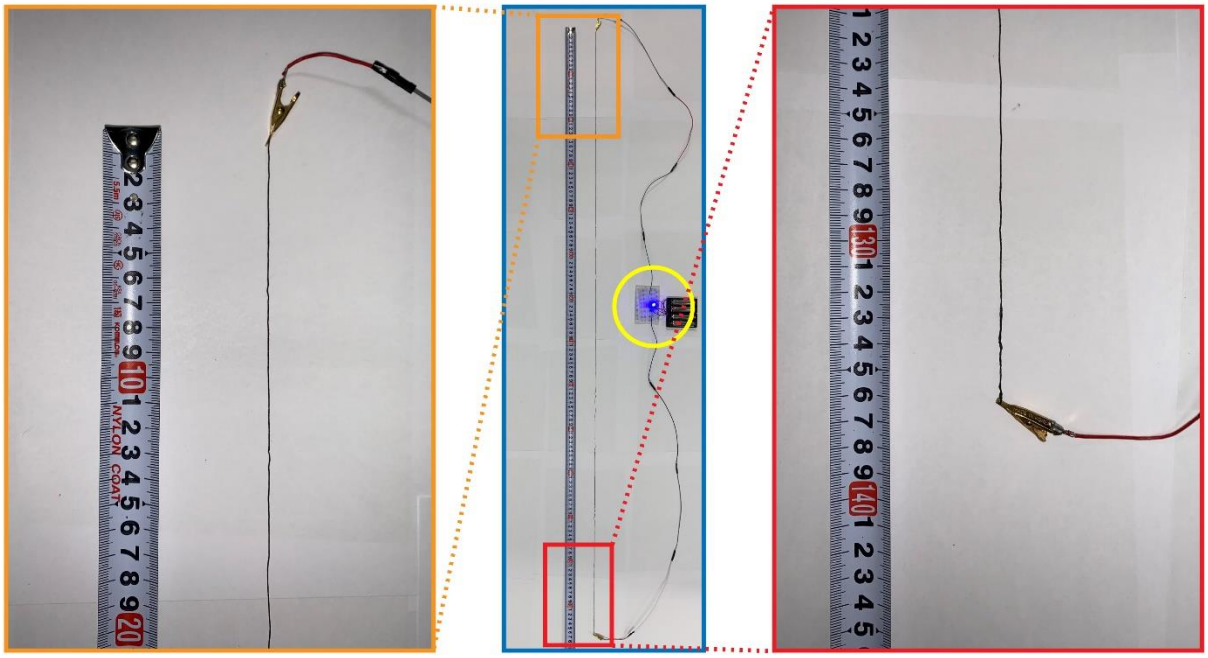

Fig. S25 Fabrication of a long TPS. 136 cm long TPS1300 was easily fabricated. The yellow circle represents blue LED light

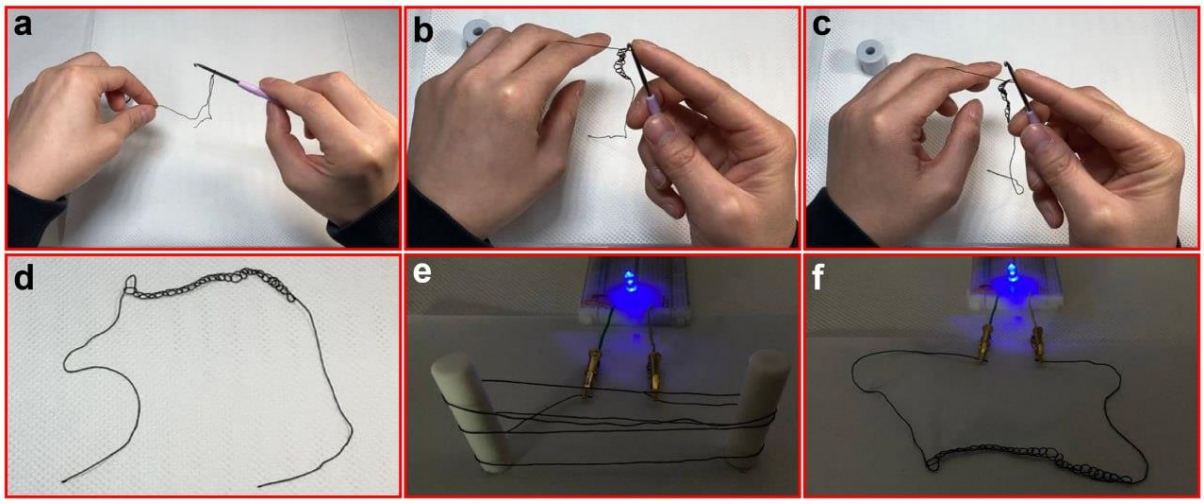

Fig. S26 Knitting with TPS1300 using superflexibility. **a** to **d** The process of knitting with TPS1300. Lighted blue LED **e** before and **f** after knitting

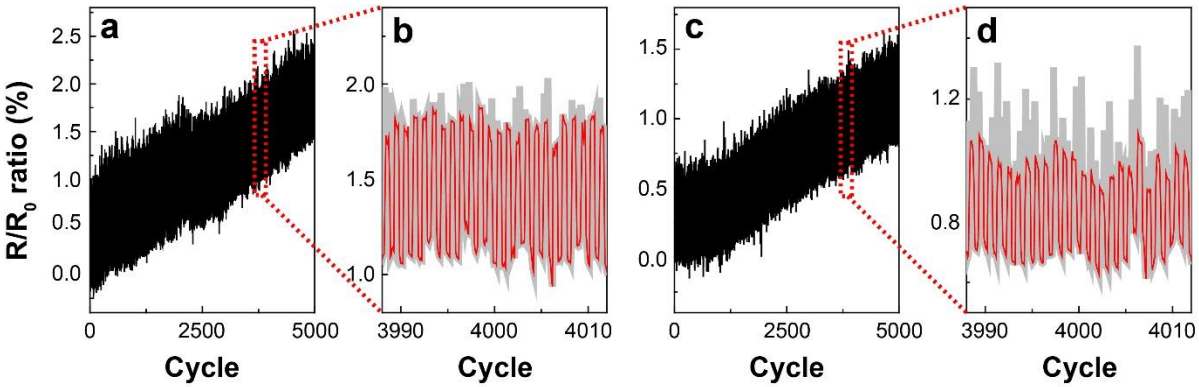

Fig. S27 Bending cycle-dependent resistance of TP cotton and TP wool treated at 900 °C. Resistance variation during 5000 bending cycles for **a**-**b** TP cotton and **c**-**d** TP wool

We measured 5000 bending-cycle dependent R (Fig. S27). The variations in R/R_0 of TP900 are about 0.8% for TP cotton (Fig. S27a and b) and 0.4% for TP wool (Fig. S27c and d). Although these values are comparable with TPS (0.6%), the R of TP cotton and TP wool continuously increase (Fig. S27a and c). Moreover, both fabrics were not stable for grabbing (Movie S5), even heat-treated at 900 °C.

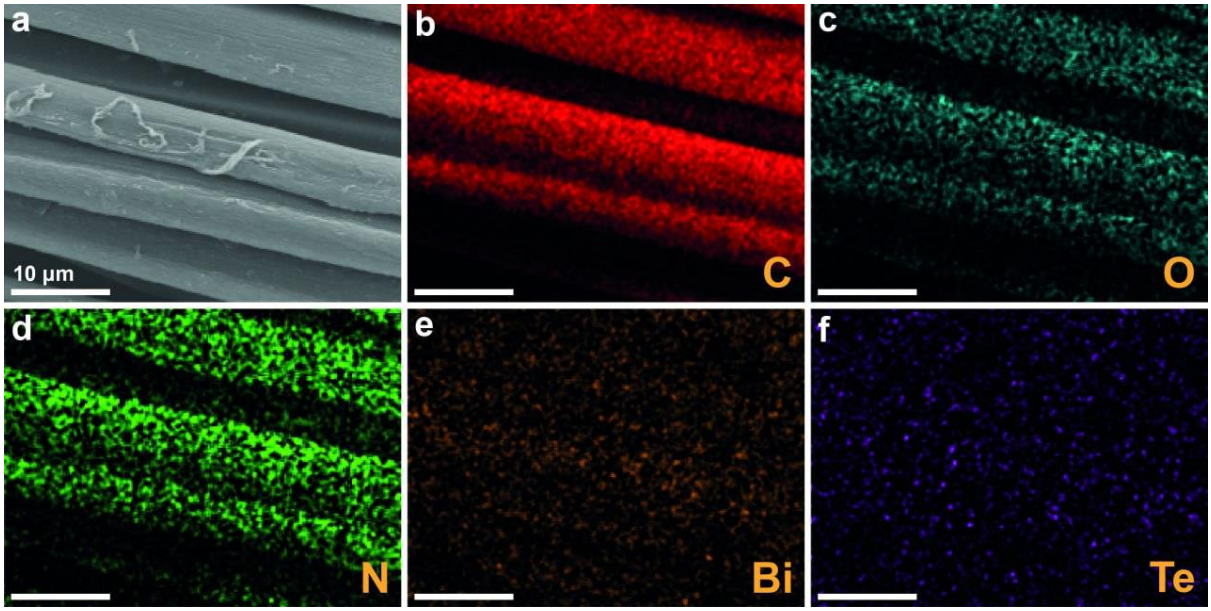

Fig. S28. SEM study of Bi_2Te_3-coated TPS. **a** SEM image of Bi_2Te_3-coated TPS thermally treated at 550 °C. **b-f** EDS elemental mapping of C, O, N, Bi, and Te, respectively. All scale bars are 10 µm

Table S1. Decrease in fiber diameter ratio

Sample	Pristine (μm)	HT 900 ℃ (μm)	Ratio (%)	PDA-coated (μm)	TP 900 ℃ (μm)	Ratio (%)
Silk	11.0	6.31	42.4	11.9	5.19	56.2
Cotton	11.6	6.50	43.7	12.7	8.44	33.3
Wool	16.0	7.77	51.4	17.0	10.2	40.1
Hemp	18.8	9.08	51.6	23.2	15.9	31.6

Table S2. Raman bands of TPS

Peak		HTT (°C)								
		800	**900**	**1000**	**1100**	**1200**	**1300**	**1350**	**1400**	**1450**
D₄	**Position (cm^{-1})**	1237	1206	1229	1248	1259	1242	1234	1233	1221
	FWHM (cm^{-1})	234	200	221	244	242	227	247	214	230
	Ratio (%)	21.20	15.00	15.82	17.41	17.61	12.83	11.25	8.65	7.86
D	**Position (cm^{-1})**	1368	1357	1360	1359	1347	1347	1352	1342	1340
	FWHM (cm^{-1})	169	164	149	138	109	102	124	80	137
	Ratio (%)	38.57	44.10	42.62	41.16	43.90	50.74	53.09	57.75	58.43
D₃	**Position (cm^{-1})**	1526	1520	1518	1523	1516	1512	1522	1520	1515
	FWHM (cm^{-1})	143	130	131	140	163	169	141	192	122
	Ratio (%)	21.49	18.28	17.47	18.56	16.10	14.43	14.13	12.02	9.15
G	**Position (cm^{-1})**	1604	1603	1607	1606	1604	1604	1607	1603	1601
	FWHM (cm^{-1})	87	82	87	81	76	78	92	71	109
	Ratio (%)	16.74	21.62	23.07	21.91	22.03	21.64	21.53	21.57	24.56
D₂	**Position (cm^{-1})**	1679	1684	1695	1678	1699	1704	1698	1701	1737
	FWHM (cm^{-1})	103	75	90	96	75	78	50	50	50
	Ratio (%)	2	0.99	1.03	0.96	0.36	0.35	0.00	0.00	0.00
D₄+D	**Position (cm^{-1})**	2521	2518	2481	2498	2482	2486	2462	2481	2468
	FWHM (cm^{-1})	340	345	276	293	253	186	266	192	176
	Ratio (%)	28.07	24.71	22.39	18.23	15.97	16.23	26.21	10.25	10.17
2D	**Position (cm^{-1})**	2724	2725	2699	2699	2680	2673	2664	2664	2643
	FWHM (cm^{-1})	287	273	254	249	218	202	206	157	169
	Ratio (%)	36.70	37.30	37.83	40.20	42.20	44.08	50.84	58.25	51.72
D+G	**Position (cm^{-1})**	2914	2917	2921	2918	2911	2911	2891	2908	2882
	FWHM (cm^{-1})	237	214	229	218	199	188	197	168	222
	Ratio (%)	27.46	28.79	34.46	34.00	36.24	34.81	22.43	28.4	34.77
2D₂	**Position (cm^{-1})**	3112	3121	3157	3141	3153	3165	3094	3177	3173
	FWHM (cm^{-1})	207	206	157	190	157	169	68	146	147
	Ratio (%)	7.77	9.20	5.31	7.57	5.59	4.88	0.52	3.10	3.34

Table S3. XPS spectra of TPS

Element	Chemical species		HTT (°C)								
			800	900	1000	1100	1200	1300	1350	1400	1450
C1s	C = C (sp^2)	Position (eV)	284.50	284.50	284.50	284.50	284.50	284.50	284.50	284.50	284.50
		FWHM (eV)	1.23	1.14	1.19	1.14	1.10	1.08	1.04	1.10	0.99
		Ratio (%)	35.71	37.36	41.74	46.92	51.91	52.77	55.40	56.90	57.87
	C – C (sp^3)	Position (eV)	285.19	285.11	285.14	285.17	285.55	285.54	285.36	285.71	285.78
		FWHM (eV)	2.35	2.37	2.50	2.33	2.24	2.30	2.56	2.05	2.35
		Ratio (%)	40.35	39.90	38.05	32.35	27.43	24.82	24.00	23.33	23.76
	C-O C-OH C-N	Position (eV)	287.37	287.37	287.25	286.99	287.39	287.17	287.00	287.48	287.83
		FWHM (eV)	2.10	2.21	2.02	2.08	1.79	2.29	2.30	1.56	1.35
		Ratio (%)	9.39	9.81	7.37	6.86	5.48	5.91	5.10	5.03	4.38
	C=O O-C=O	Position (eV)	289.28	289.20	288.92	288.58	288.78	288.74	288.50	289.01	289.32
		FWHM (eV)	2.29	2.65	2.26	2.46	2.26	2.24	2.30	2.20	2.12
		Ratio (%)	11.05	8.06	5.23	5.09	4.95	4.36	4.29	4.77	4.84
	$\pi - \pi^*$ shake up feature	Position (eV)	291.55	291.36	290.80	290.54	290.75	290.62	290.69	290.88	291.31
		FWHM (eV)	2.53	2.72	3.21	3.49	3.00	3.18	3.40	2.86	3.20
		Ratio (%)	3.50	4.88	7.60	8.78	10.23	12.13	11.22	9.97	9.15
O1s	Na KLL	Position (eV)	535.79	535.64	535.98	-	-	-	-	-	-
		FWHM (eV)	3.02	3.30	2.15	-	-	-	-	-	-
		Ratio (%)	19.93	18.93	10.47	-	-	-	-	-	-
	C = O	Position (eV)	532.90	533.11	533.03	532.29	532.28	532.29	531.11	531.92	530.97
		FWHM (eV)	3.61	3.13	2.17	2.49	2.65	2.50	3.37	2.36	3.11
		Ratio (%)	23.80	29.54	34.07	42.36	86.30	100.00	395.05	100.00	100.00
	C - O	Position (eV)	531.07	530.55	531.64	530.95	529.90	-	-	-	-
		FWHM (eV)	2.23	2.66	2.81	2.31	2.42	-	-	-	-
		Ratio (%)	76.20	70.46	65.93	57.64	13.70		-		-
N1s	Pyridinic	Position (eV)	398.11	398.02	-	-	-	-	-	-	-
		FWHM (eV)	1.34	1.45	-	-	-	-	-	-	-
		Ratio (%)	17.62	6.32	-	-	-	-	-	-	-
	Pyrrolic	Position (eV)	400.73	400.99	401.23	401.20	401.60	-	-	-	-
		FWHM (eV)	2.15	2.06	2.50	2.05	2.56	-	-	-	-
		Ratio (%)	68.08	80.10	100.00	100.00	100.00	-	-	-	-
	Oxidized	Position (eV)	403.99	404.85	-	-	-	-	-	-	-
		FWHM (eV)	3.57	3.12	-	-	-	-	-	-	-
		Ratio (%)	14.30	13.58	-	-	-	-	-	-	-

Table S4. XPS spectra of pristine silk and PDA-coated Silk

Element	Chemical species		Pristine Silk	PDA-coated Silk
C1s	C = C (sp^2)	Position (eV)	284.50	284.50
		FWHM (eV)	1.92	1.89
		Ratio (%)	8.99	7.91
	C – C (sp^3)	Position (eV)	285.56	285.87
		FWHM (eV)	1.48	1.77
		Ratio (%)	28.32	46.63
	C-O C-OH C-N	Position (eV)	286.89	287.32
		FWHM (eV)	1.77	1.68
		Ratio (%)	34.71	22.52
	C=O O-C=O	Position (eV)	288.79	288.91
		FWHM (eV)	1.87	2.30
		Ratio (%)	23.41	18.76
	COOH	Position (eV)	290.24	290.86
		FWHM (eV)	2.68	3.23
		Ratio (%)	4.57	4.17
O1s	O-C=O	Position (eV)	533.94	-
		FWHM (eV)	2.21	-
		Ratio (%)	21.74	-
	C = O	Position (eV)	532.29	533.82
		FWHM (eV)	2.12	2.60
		Ratio (%)	73.27	56.50
	C - O	Position (eV)	530.18	532.30
		FWHM (eV)	1.50	2.16
		Ratio (%)	4.99	43.50
N1s	Pyridinic	Position (eV)	402.30	402.73
		FWHM (eV)	2.20	2.15
		Ratio (%)	10.05	18.12
	Pyrrolic	Position (eV)	400.70	400.92
		FWHM (eV)	1.82	1.89
		Ratio (%)	83.09	70.93
	Oxidized	Position (eV)	399.18	399.33
		FWHM (eV)	1.84	1.38
		Ratio (%)	6.86	10.95
I3d	$I3d_{3/2}$ B	Position (eV)	-	633.08
		FWHM (eV)	-	1.95
		Ratio (%)	-	28.47
	$I3d_{3/2}$ A	Position (eV)	-	630.91
		FWHM (eV)	-	2.03
		Ratio (%)	-	11.80
	$I3d_{5/2}$ B	Position (eV)	-	621.59
		FWHM (eV)	-	2.13
		Ratio (%)	-	48.90
	$I3d_{5/2}$ A	Position (eV)	-	619.36
		FWHM (eV)	-	1.72
		Ratio (%)	-	10.83

References

[S1] Proniewicz LM, Paluszkiewicz C, Wesełucha-Birczyńska A, Majcherczyk H, Barański A, Konieczna A (2001) FT-IR and FT-Raman study of hydrothermally degradated cellulose. J Mol Struct 596**:**163-169.

[S2] Hogg LJ, Edwards HGM, Farwell DW, Peters AT (1994) FT Raman spectroscopic studies of wool. J Soc Dye Colour 110:196-199.

[S3] Uematsu H, Kawasaki T, Koizumi K, Yamaguchi A, Sugihara S, Yamane M, Kawabe K, Ozaki Y, Tanoue S (2021) Relationship between crystalline structure of polyamide 6 within carbon fibers and their mechanical properties studied using Micro-Raman spectroscopy. Polymer 223:123711.

[S4] Monti P, Freddi G, Bertoluzza A, Kasai N, Tsukada M (1998) Raman spectroscopic studies of silk fibroin from Bombyx mori. J Raman Spectrosc 29:297-304.

[S5] Schwan J, Ulrich S, Batori V, Ehrhardt H, Silva SRP (1996) Raman spectroscopy on amorphous carbon films. J Appl Phys 80:440-447.

[S6] Krauss B, Lohmann T, Chae DH, Haluska M, von Klitzing K, Smet JH (2009) Laser-induced disassembly of a graphene single crystal into a nanocrystalline network. Phys Rev B 79:165428.

[S7] Lee JY, Kim NY, Shin DY, Park H-Y, Lee S-S, Kwon SJ, Lim D-H, Bong KW, Son JG, Kim JY (2017) Nitrogen-doped graphene-wrapped iron nanofragments for high-performance oxygen reduction electrocatalysts. J Nanoparticle Res 19:98.